Earth and Planetary Science Letters 273 (2008) 195–202

Contents lists available at ScienceDirect

Earth and Planetary Science Letters

journal homepage: www.elsevier.com/locate/epsl

Thermal history, partial preservation and sampling bias recorded by Stardust cometary grains during their capture

Mathieu Roskosz [a,*], Hugues Leroux [a], Heather C. Watson [b]

[a] Laboratoire Structure et Propriétés de l'Etat Solide, Université des Sciences et Technologies de Lille, CNRS, UMR 8008, 59655 Villeneuve d'Ascq, France
[b] Lawrence Livermore National Laboratory, Earth and Environment, 7000 East Avenue L-206, Livermore CA 94550, USA

ARTICLE INFO

Article history:
Received 8 April 2008
Received in revised form 23 June 2008
Accepted 23 June 2008
Available online 3 July 2008

Editor: R.W. Carlson

Keywords:
cometary dusts
Stardust
melts
diffusion
thermal history

ABSTRACT

The nature and origin of cometary grains are poorly known. For this reason the first *in situ* sampling of cometary materials, the Stardust mission, raised considerable expectations. The Stardust spacecraft captured cometary dusts at a relative velocity of 6.1 km/s in a low density silica aerogel medium. Calculations and laboratory experiments on the shock behaviour of aerogel and hypothetical dust-analogue material indicate that an intense but short heating stage (on the order of the microsecond) occurred during the collection; however, results from the preliminary team emphasized that a large fraction of the collected material was deeply affected by the thermal event, indirectly suggesting that the heating was more protracted. Here we constrain its parameters based on diffusion of MgO and SiO_2 between a molten cometary dust and the embedding molten aerogel. After the shock, this assemblage stayed at ~2100 K for duration of up to 0.1 ms. This timescale is characteristic for friable and fine-grained aggregates whereas consolidated grains were quenched faster. Therefore, a sampling bias occurred during the collection. It may explain the recent finding that preserved cometary grains look more similar to inner solar nebula material than to chondritic porous interplanetary dust particles (CP-IDP). Indeed, CP-IDPs and other primitive materials are friable materials and consequently, they must have been selectively damaged. The strong thermal modification precludes detailed studies of mineralogy, but molten cometary dusts are only partially mixed with aerogel, giving an opportunity to analyze bulk and local compositions of the impacting aggregate fragments.

1. Introduction

Cometary dust particles are generally described as relicts of pristine materials that accreted to form primitive meteorites and planets. Compared to other small primitive objects of the solar system these grains are poorly known, yet they may be the only mineralogical objects unaltered since the formation of the Solar nebula. They also may represent a crucial hidden 'reservoir' able to explain some major processes which occurred during the early evolution of the Earth, such as the delivery of water (Zolensky, 2005). In this respect, the first *in situ* sampling of cometary materials, the Stardust mission, raised considerable expectations from astrophysicists, geologists, mineralogists and cosmochemists. Indeed, these dusts are the unique and undisputable comet samples available so far to investigate the nature of cometary materials. The Stardust mission was a plain success but still had to face inherent problems related to the collection of samples itself. They were captured from the 81P/Wild 2 comet tail at a relative velocity of 6.1 km/s in a low density silica aerogel medium. After this hypervelocity impact, flash-heating of dust grains could not be avoided. Our vision of cometary materials is blurred by this thermal event and must be corrected by knowing the thermal history of the sample collection. Based on diffusion of MgO and SiO_2 between a molten cometary dust and the embedding molten aerogel (pure SiO_2), we derive the main parameters of this thermal event (i.e. peak temperature, duration of the pulse, cooling rate, and thermal gradients). A comparison with values determined from shock experiments reveals that a sampling bias may have happened during the collection. Compared to coarse grains, poorly cohesive aggregates have suffered considerable damage. On the other hand, our study also confirms that even completely molten relicts bear important information on the nature of the pristine cometary grains and therefore deserve particular attention from the community.

2. Analytical method

The studied sample comes from track 41, collector 2044. The sample was removed from aerogel, embedded in epoxy and sliced into 50–70 nm-thick sections with an ultramicrotome at the Johnson Space Center (NASA). Sections were then transferred to amorphous C-supported Cu TEM grids. More details about sample preparation are given elsewhere (Zolensky et al., 2006) and a general description of the sample may be found in Leroux et al. (in press).

* Corresponding author.
E-mail address: mathieu.roskosz@univ-lille1.fr (M. Roskosz).

0012-821X/$ – see front matter © 2008 Elsevier B.V. All rights reserved.
doi:10.1016/j.epsl.2008.06.033

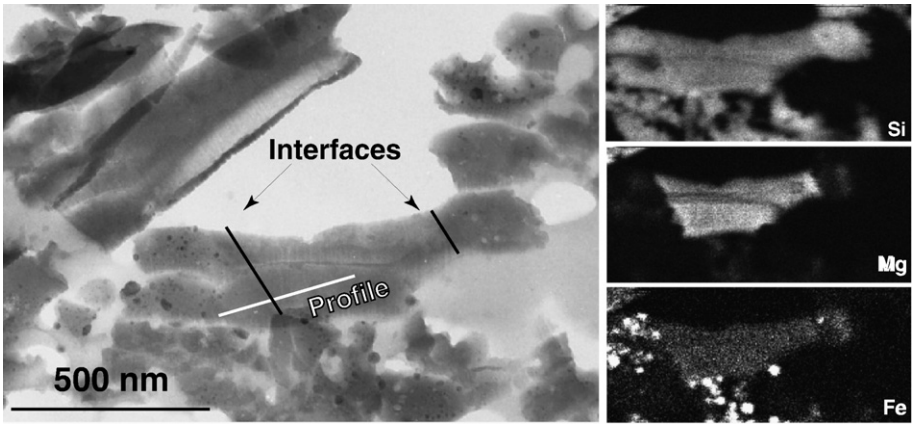

Fig. 1. TEM Bright field (left) and chemical distribution for Si, Mg and Fe (right) of the sample. The composition profile (white line here and open symbols on Fig. 2) is measured at the aerogel/"ghost mineral" interface (black lines). The latter are revealed by their high MgO concentration. The microstructure consists of a silica-rich glassy matrix containing nanometer-sized beads of Fe–Ni–S phases and vesicles. The Fe–Ni–S phases are made of Ni-bearing metal and iron-sulphide phases (see Zolensky et al., 2006 and Leroux et al., in press for details). Microanalyses show that the average composition of the sample is silica-rich, suggesting that there is a large fraction of molten aerogel. Most of the analyses performed led to compositions with 90 mol % of SiO_2 or more. On the other hand, most of the MgO-rich areas have typically 35 mol% of MgO and the composition is approximately constant within a given MgO-rich area.

The ATEM study was performed using a Tecnai G2-20 twin (LaB_6 filament) operating at 200 kV. Specimens were mounted on a beryllium low-background double-tilt holder. The microstructure was obtained by bright/dark field imaging, both in conventional direct TEM mode (parallel illumination) and in scanning (STEM) mode (convergent illumination). Chemical compositions were measured using Energy Dispersive X-ray Spectroscopy (EDS) with an EDAX Si-detector with ultrathin window. We used probe sizes ranging from 5 to 10 nm either as a fixed probe or as scanning probe for analysis of extended areas. For quantitative analyses, calculations of element concentrations and atomic ratios were carried out using calibrated *k*-factors and thin film matrix correction procedures. Data reduction was obtained using the TIA software. The absorption correction procedure was based on the principle of electroneutrality (Van Cappellen and Doukhan, 1994). The *k*-factors for O and Mg were determined using quartz and forsterite standard samples by the parameter-less method of Van Cappellen (1990). Element distributions were obtained by EDS X-ray spectral imaging. In this method, each pixel of the chemical maps contains a full EDX spectrum. Maps were recorded with an X-ray stored intensity ranging from 1000–2000 counts/s and a dwell time of 200 to 800 ms for areas extended from 200 to 400 pixels square. For the long duration experiments, we applied drift compensation and ensured a high vacuum to minimize the contamination of TEM slices. The distribution of elements was deduced from the spectra collection by selecting manually the characteristic K_α peak energy window (including background and potential tail of a nearby peak). Any individual element can be chosen after the experiment. The X-ray intensities corresponding to the elements of interest were calculated for each pixel of the map and then converted to a proportional grey level. Individual spectra had a low X-ray count because the acquisition dwell time was short; however we stacked a number of adjacent spectra in order to quantify selected area with a good count statistics. This quantification, contrary to the spatial distribution visualization, includes a background subtraction and correction (absorption and *k*-factors). The lateral resolution of an analytical spot was typically of the order of 10 nm. This setup was particularly useful to measure concentration profiles at the grain-aerogel interface.

3. Results

An overview of the mineralogy of cometary dust particles collected during the Stardust mission was recently published (Zolensky et al., 2006; Brownlee et al., 2006). A significant fraction of silicate dust was found molten and mixed with molten aerogel (Zolensky et al., 2006; Leroux et al., in press; Rietmeijer et al., in press). This effect is particularly noticeable in particles from the internal walls of tracks. To quantify one of the highest grades of thermal alteration recorded by Stardust samples, we focused on a highly thermally modified sample labeled C2044,2,41,3,6. The typical microstructure of this sample consists of a vesicular, silica-rich, glassy matrix containing nanoscale beads of Fe–Ni–S phases (Fig. 1). At the sub-micron scale compositions are highly variable and include micron-size pockets of MgO-rich glasses embedded in a SiO_2-rich matrix (Leroux et al., in press). These pockets outline ghost mineral assemblages (Fig. 1). The coexistence of these molten cometary minerals with the embedding molten aerogel provides a unique tool to establish the thermal history of grains during their capture. Only extended amorphous MgO-rich patches in contact with molten aerogel, up to 0.5 μm wide, free of vesicles and Fe–Ni–S inclusions were selected to study the inter-diffusion of MgO and SiO_2. Their MgO/(MgO+FeO) ratios are within the range 95–98% and consequently these different glasses probably originated from almost Fe-free minerals such as enstatite ($MgSiO_3$) or forsterite (Mg_2SiO_4). Because the bulk SiO_2 concentration of the glass pocket is much closer to enstatite rather than forsterite stoichiometry (see below), it appears more reasonable to consider that the initial silicate was an enstatite

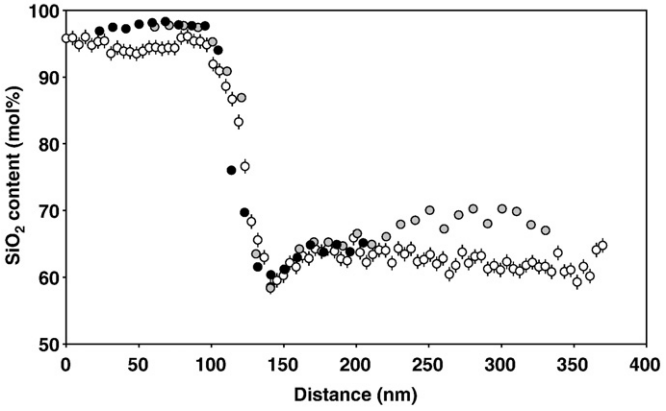

Fig. 2. Composition profiles across the interface between the SiO_2-rich matrix and a MgO-rich region. The profile in open symbols is used to derive quantitative results because it is the best resolved. The location of the white profile is shown on Fig. 1.

grain. If instead it had been a more MgO-rich forsterite grain, it would imply a larger contamination of the molten mineral by the aerogel and, as explained below, it would imply an even longer thermal pulse during the collect. Far from the interface, both MgO-rich and SiO_2-rich glasses have homogeneous compositions within the error bars (typically ±1 mol%), with an MgO content in the range 30–40 mol% and 2–5 mol% respectively (Fig. 2). This homogeneity is significant because it spreads over several hundreds of nanometers, contrasting with the relative sharpness of the apparent interface (about 50 nm). Finally, the interface shows a typical horn-like shape, particularly obvious in the MgO-rich liquid. We use this feature below to constrain the cooling rate of the grain.

4. Discussion

4.1. Liquid–liquid immiscibility in the MgO–SiO_2 phase diagram and the determination of the thermal history of molten Stardust grains

The concentration profile recorded the thermal history of the sample during collection. After the melting of a Mg-rich mineral and its surrounding aerogel, inter-diffusion of MgO and SiO_2 occurred. Melt compositions changed from 50 mol% and 100 mol% to 62.5 mol% and 95 mol% respectively (Fig. 3). The horn-like shape of the diffusion profile appeared subsequently. Typically, this feature is characteristic of an exsolution/unmixing process upon cooling. In the case of the binary system MgO–SiO_2, unmixing is related to the large liquid–liquid miscibility gap that exists in its SiO_2-rich portion (Hudon and Baker, 2002; Mysen and Richet, 2005; Leroux et al., in press). This particular shape appeared upon the continuous cooling of the sample during which compositions of the SiO_2-rich and the MgO-rich immiscible liquids changed along the two branches of the miscibility gap at the interface (Fig. 3). We used the persistence of melt pockets, the extent of the contamination of the silica matrix by MgO, and the shape of the inter-diffusion profile to shed light on the thermal history of cometary dust particles collected by the spacecraft. In this framework, compositions of the two glasses far from the interface record the temperature at which the two liquids reached their equilibrium compositions (i.e. "touched the branches of the miscibility gap on the phase diagram"), and the MgO enrichment of the MgO-rich liquid close to the interface is characteristic of the cooling rate.

4.2. Determination of the peak temperature

Based on the phase diagram (Fig. 3), two independent determinations of the temperature at which the unmixing started is obtained for MgO- and SiO_2-rich liquids respectively: ~2050 K and ~2100 K. Based on the original phase diagram, an accuracy of ±10 K may represent an upper value for the uncertainty. These internally-consistent values confirm that compositions of these liquids attained their equilibrium composition simultaneously at ~2075 K. The peak temperature determined here is the characteristic temperature from which the dust was quenched from a thermal equilibrium. Even if temperature had been slightly higher for a very short duration, it did not leave any chemical or structural imprint (Fig. 3).

4.3. Modelling diffusion profiles

The time required for the two melts to initially attain an equilibrium composition at the characteristic temperature was calculated by using an isothermal diffusion model. The cooling rate from this equilibrium stage was then determined by modelling the diffusion profile with a similar method to that used to determine cooling rates of iron meteorites exsolving kamacite from taenite (Hopfe and Goldstein, 2001). A finite difference model for diffusion in two immiscible phases undergoing cooling was employed. Concentration and temperature dependent MgO and SiO_2 diffusion coefficients were used. The partitioning behaviour at the interface was determined from the MgO–SiO_2 phase diagram (Fig. 3). Finally, the effect of a tilted interface relative to the ATEM electron beam on the shape of the profile was taken into account.

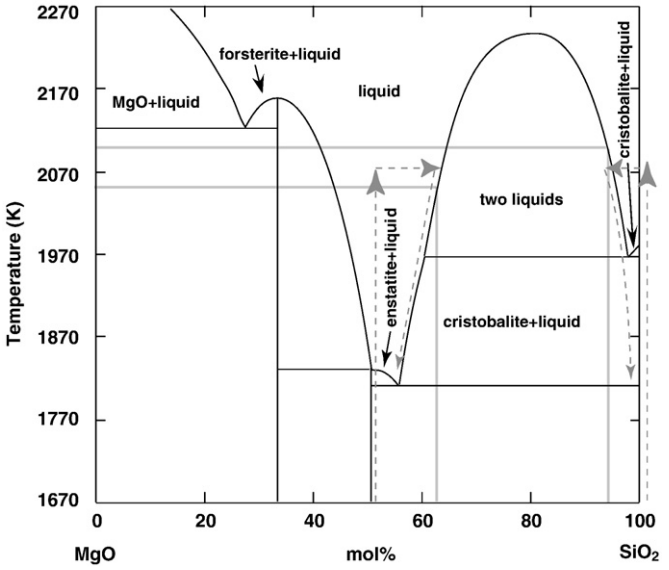

Fig. 3. Binary phase diagram MgO–SiO_2 (Based on Mysen and Richet, 2005); the schematic Composition–Temperature path followed by the cometary dust particle and its embedding aerogel are illustrated by doted arrows. After the impact, the heat released induced a rapid increase of temperature above the liquidus temperature of pure SiO_2 (dashed ascending arrows). Then, the two immiscible liquids equilibrated at a characteristic temperature by inter-diffusion of SiO_2 and MgO (dashed horizontal arrows). Compositions of the two liquids far from the interface are indicated by the grey vertical lines. Temperatures at which these two liquids co-exist is in the range of 2050–2100 K according to the MgO-rich and the SiO_2-rich liquid compositions respectively (grey horizontal lines). Finally, upon cooling, compositions of the melts changed along the two branches of the miscibility gap (descending dashed arrows).

4.3.1. Composition and temperature dependence of diffusion coefficients in the MgO–SiO_2 binary system

Diffusion coefficients for MgO and SiO_2 (D_{MgO}, D_{SiO2}) are key factors controlling the shape of the diffusion profiles. A reasonably good knowledge of this property is required to model profiles and to extract quantitative information on the cooling rate of Stardust samples. Compared to the usual situation (i.e. subsolidus chemical re-equilibration of minerals showing comparable dynamics), our study is complicated by the fact that properties of SiO_2-rich melts (typically in the range of 95–100 mol% SiO_2) depend dramatically on the melt composition. For instance, the addition of 0.05 mol% of Na_2O to pure silica induces a drop of viscosity by more than 5 orders of magnitude at 1470 K (Leko et al., 1977). Here, the two coexisting liquids have very different SiO_2 contents, one of them being higher than 95 mol% SiO_2. As a consequence, composition-dependent diffusion coefficients have to be considered in order to satisfactorily model experimental profiles.

The composition-dependence of *D*s in silicate liquids with SiO_2-content lower than 70 mol% has been documented for different silicate systems from binary CaO–SiO_2 to SiO_2–$NaAlSiO_4$ (Keller et al., 1979; Bockris et al., 1955; Toplis et al., 1997; Lacks et al., 2007). It is always found to be relatively weak (Fig. 4). As a consequence, available experimental data on haplobasaltic melts (LaTourette et al., 1996) likely describe diffusion coefficients in the MgO-rich liquid studied herein. Moreover, for this liquid, the temperature dependence is well documented over the temperature range of interest. An Arrhenian behaviour of the form $D_{MgO} = 0.198 \cdot 10^{-4} * \exp(-173\ \text{kJ/mol}/RT)$ (LaTourette et al., 1996) was used where T is temperature in K and R is the gas constant. This relationship describes

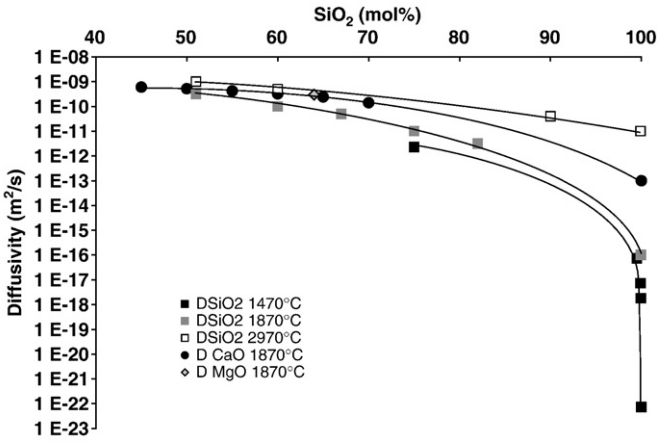

Fig. 4. Diffusion coefficients of CaO, MgO and SiO_2 as a function of SiO_2-content and temperature. D_{SiO2} was determined from viscosity data in the system Na_2O–SiO_2 (Leko et al., 1977; Toplis et al., 1997) and molecular dynamics calculation (Lacks et al., 2007). The Eyring equation, proved to relate efficiently D_{SiO2} to the bulk viscosity in SiO_2-rich liquids (LaTourette et al., 1996) was employed. The effect of substituting Na_2O for MgO is negligible compared to the effect of adding any network-modifying cation to pure molten silica. D_{CaO} in SiO_2-poor liquids are from Keller et al. (1979) and data for SiO_2-rich liquids are from Toplis et al. (1997). At a given SiO_2-content and at 1870 K, it is experimentally shown that D_{CaO}–D_{MgO}. Data for MgO are from LaTourette et al. (1996). Lines are only guides for the eyes.

the diffusion of MgO in the MgO-rich liquid. Moreover, compositional variations close to the interface, in this liquid, should not result in significant variations of D_{MgO}.

The SiO_2-rich liquid is more complicated to describe because experimental data are not directly available for MgO as a minor element but the few data available for CaO were used to approximate D_{MgO} in SiO_2-rich liquids (Fig. 4). This approximation is reasonable since LaTourette et al. (1996) showed that *D*s for CaO and MgO were comparable within error bars at comparable cation concentrations and temperatures. There is also limited data on diffusivity of SiO_2 at high temperature. An approximation for the temperature and composition effects on SiO_2 diffusion was made from viscosity measurements and molecular dynamics simulations of SiO_2 diffusion at 1873 K and 3000 K respectively (Toplis et al., 1997; Lacks et al., 2007). Each set of data describes the compositional effect on D_{SiO2}, and their difference, in essence, provides an estimate of the activation energy. The following relationship was determined to describe D_{SiO2} at the higher SiO_2 concentrations: $D_{SiO2}=1\cdot10^{-5}*\exp(0.1236*\mathrm{Conc}_{SiO2})*\exp(-70\ \mathrm{kJ/mol}/RT)$, where Conc_{SiO2} is the concentration at a given point in the profile, T is the temperature (K), and R is the universal gas constant (Fig. 4).

Fortunately, the inherently large uncertainties in this determination do not affect the general outcome of the measurements, as the most "information-rich" part of the profile is the MgO-rich side. In both cases, the determination of diffusion coefficients is somewhat uncertain. For MgO the coefficients used are probably valid within a factor of two, which does little to change the suggestion that the two melts experienced a heating event persisting for a time-scale on the order of 0.1 ms (see below). Finally, due to the large composition-dependence of D_{SiO2} in SiO_2-rich liquids, large uncertainties are expected and consequently, we focussed our efforts on fitting the MgO-rich portion of the profiles.

4.3.2. Diffusion profile model

The model utilizes an explicit finite difference approximation for one-dimensional diffusion across two distinct phases, undergoing linear cooling (or no cooling, as in the isothermal case). The concentration profiles are set up as one-dimensional arrays, consisting of N spatial elements of a constant size, dX (1 nm). This method calculates the flux in and out of each dX element (i) by the gradient in concentration between the two (i.e. Fick's first law, Crank, 1975). This can be expressed by:

$$C_{i,t+1} = C_{i,t} + D_i\left(C_{i-1,t}-C_{i,t}\right)\frac{\mathrm{d}t}{\mathrm{d}X^2} + D_i\left(C_{i+1,t}-C_{i,t}\right)\frac{\mathrm{d}t}{\mathrm{d}X^2}, \quad (1)$$

where D is the diffusion coefficient in element i, dt is the time-step, $C_{i,t}$ is the concentration in element i, at the new time, $C_{i,t-1}$ is the concentration at the previous time-step. Therefore, the new concentration (time = t+1) is equal to the old concentration (time = t) plus the flux in, minus the flux out.

Special consideration is given to the interface between the two phases, as well as to the end points. The flux across the boundary can be determined through knowledge of the partition coefficient, as well as the gradients one element over on each side of the boundary. This yields the following expression, where PT represents the partition coefficient of SiO_2 (ratio of SiO_2 in the MgO-rich melt to the SiO_2 rich melt), m represents element immediately to the SiO_2 side of the interface, m+1 is the element immediately on the MgO-rich side of the interface, and D_m, and D_{m+1} represent the diffusivities in phases on either side of the boundary.

$$\mathrm{FLUX} = \frac{\mathrm{PT}\left(C_{m,t} + D_m\left(C_{m-1,t}-C_{m,t}\right)\frac{\mathrm{d}t}{\mathrm{d}x^2}\right) - C_{m+1,t} - D_{m+1}\left(C_{m+2,t}-C_{m+1,t}\right)\frac{dt}{dx^2}}{1+\mathrm{PT}}, \quad (2)$$

No flux boundaries have been imposed both ends of the profile to account for the effects of impingement, (other phases growing from either side of the calculated profile). The size of dX (spatial element) is chosen as 1 nm. The value of dt (time-step) is calculated through the relation $\mathrm{d}t = R*\mathrm{d}x^2/D_N$ where R is a constant that must remain less than ~0.4 in order to maintain program stability.

The simulation begins by setting up an initial concentration step profile based on knowledge of the initial equilibrium concentrations at the starting temperature. The starting temperature was assumed to be 2075 K extracted from the flat portions of each profile as described in the next section. At each time-step, the temperature changes as a result of cooling and the time elapsed (except in the isothermal case), new diffusion coefficients are calculated for MgO and SiO_2 in both phases, new partition coefficients are calculated based on the phase diagram, and finally, new concentrations are calculated for each of the cells, depending on the gradients between them and the new parameters. This procedure is repeated until the temperature reaches below 1693 K, at which point the simulation ends. In all cooling rate models, N was chosen to be 300, and the interface was placed at N=144. This corresponds to a melt pocket of ~312 nm, although in

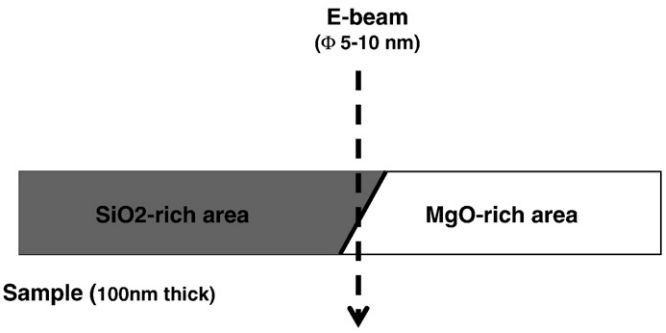

Fig. 5. Configuration of TEM-EDS analyses when the interface is not oriented parallel to the electron beam. Within a narrow central region, the electron beam convolutes different parts of the interface, resulting in an apparent continuous compositional gradient at the interface.

all models diffusion was not fast enough to reach the end of the profile and be affected by impingement.

4.3.3. Modelling the effect of the interface geometry

Composition profiles recorded by TEM-EDS showed that interfaces between the Mg-rich and Mg-poor regions are sharp but are not discontinuities as expected from the modeling approach. Analytical conditions likely explain the apparent profile at these interfaces (Fig. 5). Since each side of the interfaces is made of amorphous materials, it was not possible to move the interface parallel to the electron beam, as usually done for crystalline materials. This is not a major problem because reconstruction of the measured profile from diffusion models is easily amenable.

4.4. Quantitative parameters and thermal gradients recorded by the cometary dust

In the model, unmixing begins at 2075 K (the average of the two temperatures predicted by the end compositions) and we find that simulated profiles stop changing noticeably below ~1760 K. At this temperature, even the MgO-rich liquid is already significantly supercooled and viscous, and the viscosity of silica liquid is higher than 10^9 Pa s (Urbain et al., 1982), which prevents significant diffusion to occur below this temperature. From the initial liquid state, the assemblage was heated above 1760 K for ~0.1 ms (Fig. 6a, b, c, d). The majority of this time was spent at ~2075 K, as the MgO-rich side requires about 0.07 ms to 0.09 ms to achieve a concentration close to the measured value, assumed to be the equilibrium value. The subsequent cooling along the branches of the miscibility gap occurred relatively fast. From the model, the best fit cooling rate was of about 100 mK/s and the grain reached the "quench" temperature of ~1750 K in about 3 µs. The effect of a tilted interface on the shape of the profile is shown in Fig. 6d for angles varying from 0 to 40°. An interface tilted at about 20° likely explains the composition profile measured experimentally. Interestingly, critical features of the profile (the MgO horn and compositions far from the interface) are not significantly affected. A tilted interface also explains the absence of any SiO_2 horn in the silica-rich region of the measured profile.

Concerning thermal heterogeneity within the sample, it does not appear to be larger than 130 K. This result is based on the other concentration profiles measured on the same sample at 0.5 and 2 µm from the main profile (Figs. 2 and 7). The similarities of these profiles (shapes and mean compositions) indicate comparable thermal histories. Moreover, for these profiles, we extracted peak temperatures from the composition of the two coexisting liquids. In the first case, a temperature range of 2000–2100 K was determined. In the second case, the composition of the SiO_2-rich glass corresponds to that of a liquid at the bottom of the SiO_2-rich branch of the miscibility gap, and translates into a temperature of 1970 K (Fig. 3). This low thermal gradient is completely consistent with the protracted nature of the flash-heating, because in such conditions, temperature had the time to homogenise through the sample.

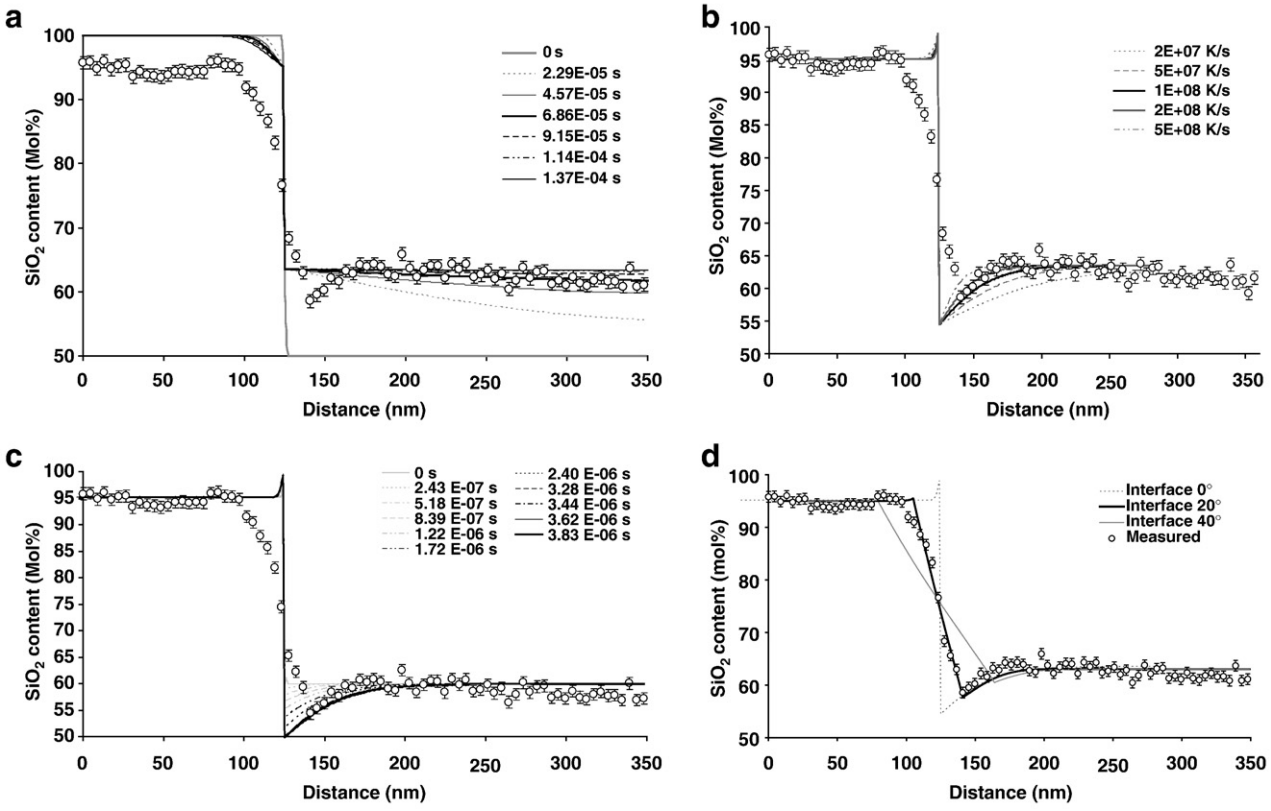

Fig. 6. a: Changes of the concentration profiles as a function of time (in seconds) at 2050 K. The profile is simulated as the others but with a cooling rate of zero. In this model $N=400$ and the interface remains at $N=144$ which corresponds to a total length of the MgO-rich portion of the profile of 256 nm, which is half of the assumed melt pocket size (512 nm). This is the upper limit of melt pockets examined, and so the equilibration time represents an upper bound on the length of time the two melts co-existed at the peak temperature. The beginning compositions are assumed to be pure enstatite and SiO_2. The time needed for the MgO-rich side to attain full equilibrium is approximately 0.15 ms, although the time it takes to attain a profile that is comparable to the one measured (within error) is between 0.07 and 0.09 ms. It should also be noted that for a smaller melt pocket (312 nm in diameter) equilibrium may be achieved after 0.03–0.05 ms. b: Simulated profiles for several cooling rates in K/s, compared to the measured data from profile 1 with a starting temperature of 2075 K. The best fit appears to be between 100 mK/s and 200 mK/s. c: The evolution with time (in seconds) of the simulated profile starting from equilibrium of both liquids at 2075 K with a cooling rate of 100E6 K/s. Below approximately 1750 K, there is little change in the profile, and it can be considered quenched. The time needed to cool down to this temperature is approximately 3 µs at this cooling rate. d: Comparison between experimental data and the calculated profile assuming a tilted interface of 0, 20 and 40°.

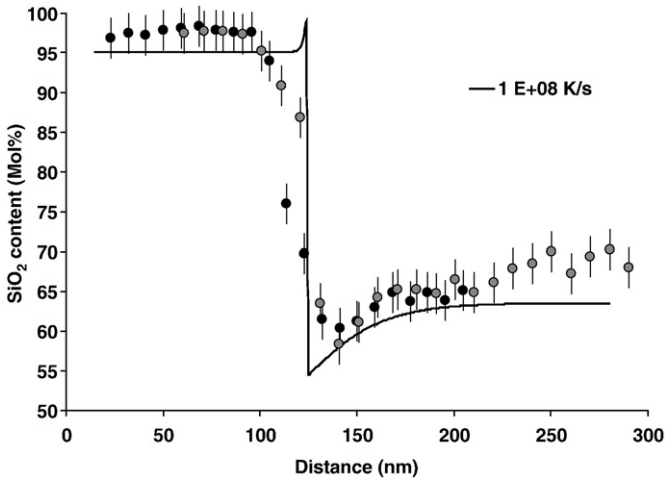

Fig. 7. Comparison of the two other profiles shown in Fig. 2 to a cooling rate simulations starting at 2075 K with a cooling rate of 100 mK/s. Although the measured data in these two profiles are not as precise as those in profile 1, it can be seen that identical starting conditions and cooling rates fit the measured profiles reasonably well. Indicative error bars are set to ±2 mol%. Real error may even be larger.

4.5. Nature of the shock, nature of the pristine material and potential sampling bias during the collect of cometary particles

For a micron-sized cometary dust, even a tenth of a millisecond is a long enough time over which considerable modifications may occur such as melting, thermal breakdown of carbonates and phyllosilicates, modification of organic matter, and chemical reactions in silicate melts. Undoubtedly, the thermal history of Stardust grains may account for some preliminary results on organics and on the occurrence of (Fe, Ni, S) droplets (Zolensky et al., 2006; Sandford et al., 2006; Leroux et al., in press). At 2100 K during 0.1 ms, a moderate production of reducing gas (e.g. carbon monoxide) from combustion of organics could locally lower the oxygen fugacity down to the IW buffer and induce the exsolution of metal droplets from FeO-bearing parent minerals. This mechanism is also consistent with the distribution of PAHs (polycyclic aromatic hydrocarbons) in the aerogel that resemble pyrolysis products of meteoritic macromolecular organics (Sandford et al., 2006). On the other hand, even the highly thermalized sample C2044,2,41,3,6 retained remarkable features of the original cometary aggregate. First, it kept a moderately angular shape (Fig. 1), which is unusual for molten materials. The mechanical properties of aerogel, its compaction during the shock and the formation of a viscous layer of molten silica at the interface between the molten dust and the compacted aerogel, helped to preserve the shape of grains. Moreover, the chemistry of grains is also partially preserved because the miscibility gap prevented MgO-bearing minerals from dissolving entirely in the molten silica. Then, despite the loss of crucial features, such grains remain a source of important mineralogical and cosmochemical information (Leroux et al., in press).

Our sample is a typical side-track particle that embodies a large fraction of the collected material (Flynn et al., 2006). They are typically constituted by silica-rich glass made of molten cometary material intermixed with molten aerogel (Leroux et al., in press). This material is found as isolated patches of "ghost" mineral assemblages distributed within the silica-rich glassy matrix (Figs. 1 and 8). In this respect, they contrast with relatively coarse-grained and cohesive impactors that survived to the track termini without strong thermal effects (Zolensky et al., 2006; Hörz et al., 2006). The former configuration demonstrates that incoming particles disaggregated during the deceleration stage into aerogel according to experiments performed before the mission (Westphal et al., 2004) and were thus likely constituted of loosely bound, friable, poorly cemented and/or highly porous aggregates (Fig. 8). Typically, when such a particle hits an aerogel cell, a shock wave is generated and induces compression and melting of aerogel. Shortly after, a flow of shocked foam comprising a viscous boundary layer forms at the surface of the particle (Sandford et al., 2006). At this point, the incoming particle disaggregates and is impregnated by molten aerogel (impregnation is likely related to the accretion stage reported in experimental and modelling approaches in Barrett et al., 1992; Hörz et al., 2000; Domínguez et al., 2004). The fast deceleration leads to strong heating of the dust fragments because the incident kinetic energy is converted on a short length scale. The full dispersion of the particle is precluded by the high viscosity of molten silica which, in addition, favours the melting of fragments. The deceleration is thus dominated by a viscous drag of a particle covered by a molten aerogel cap (Barret et al., 1992), which is probably responsible for the high temperature and the prolonged thermal history experienced by the grains. It is a consequence

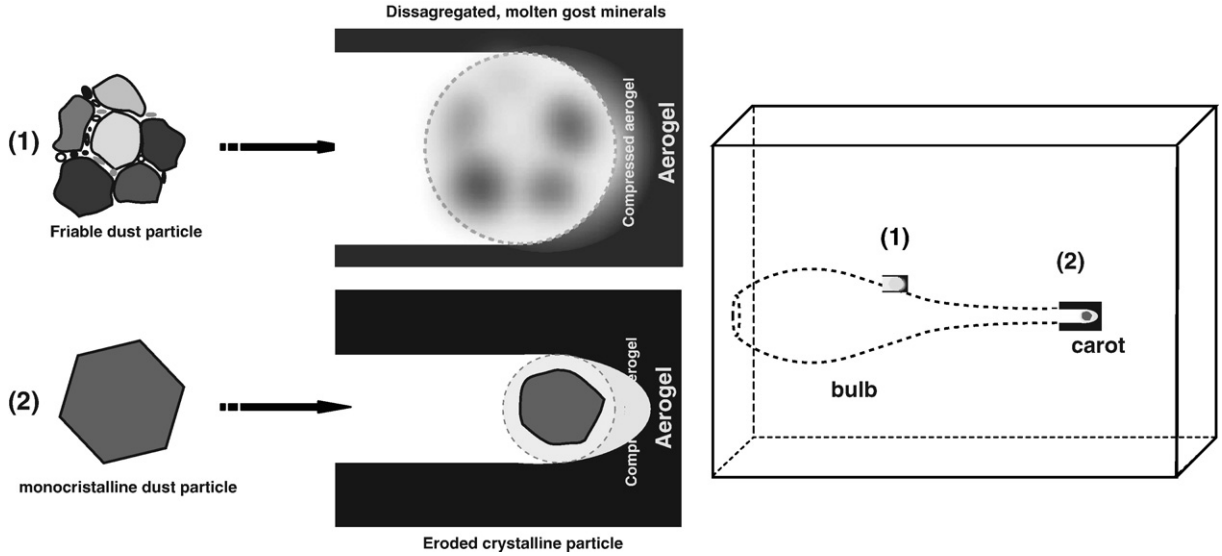

Fig. 8. Schematic relationships between dust microstructures, dominant alteration processes and location along a track. (1) friable, fine-grained aggregates, (2) dense, coarse monocrystalline particle.

of the insulator behaviour of aerogel, silica, and more generally of silicate glasses and melts, even compared to any crystalline silicate (Snyder et al., 1994; Pertermann et al., in press).

5. Conclusions

Present data shed light on unanticipated characteristics of the flash-heating of cometary dust samples. In particular the characteristic duration of the thermal event is much longer and thermal gradients are much lower than what was found experimentally on large analogue samples (Noguchi et al., 2007) or for grains at the track termini (Zolensky et al., 2006). Such particles should survive disaggregation because in this case, heating of the grain rim by friction followed by its fast abrasion must be the process controlling heat dissipation (Anderson and Arhens, 1994). This process leads to the preservation of the inner part of the particle, to the formation of large thermal gradients through the sample and to its fast cooling. In contrast, most of the thermally modified grains show clear evidence for a large dispersion into melted aerogel of fine-grained components and/or poorly cohesive aggregates, possibly comparable with CP-IDPs, which suffered considerable damage caused by impregnation of molten aerogel. The selective disaggregation and thermal modification of this dust category could explain the apparent low amount of primitive material in the comet 81P/Wild 2 (Ishii et al., 2008) because it likely caused a sampling bias. This view is also consistent with the noble gas signature reported by Marty et al. (2008) on a Stardust sample extracted from the same bulbous wall of track #41 as ours. In such highly thermalized samples, they measured very primitive and unique helium and neon signatures that definitely contrast with signatures expected for asteroidal materials. Clearly, despite the analytical challenge that represents such a study, such particles may be one of the most valuable components of Stardust samples and deserve particular attention from the community.

Acknowledgements

This study was supported by the Centre National d'Etudes Spatiales (CNES) and the electron microscope facility by European FEDER and region Nord-Pas-de-Calais. Keiko Nakamura-Messenger is gratefully acknowledged for the preparation of the ultramicrotomed TEM sample. The comments of two anonymous reviewers significantly improved the manuscript. This work performed under the auspices of the U.S. Department of Energy by Lawrence Livermore National Laboratory under Contract DE-AC52-07NA27344 (LLNL-JRNL-404716).

References

Anderson, W.W., Arhens, T.J., 1994. Physics of spacecraft-based interplanetary dust collection by impact into low-density media. LPI Technical Report 94-05, pp. 16–21.

Barrett, R.A., Zolensky, M.E., Hörz, F., Lindstrom, D., Gibson, E.K., 1992. Suitability of SiO_2 aerogel as a capture medium for interplanetary dust. Lunar Planet. Sci. 22, 203–212.

Bockris, J.O.M., Mackenzie, J.D., Kitchener, J.A., 1955. Viscous flow in silica and binary liquid silicates. Trans. Faraday Soc. 48, 75–91.

Brownlee, D., Tsou, P., Aléon, J., Alexander, C.M.O'D., Araki, T., Bajt, S., Baratta, G.A., Bastien, R., Bland, P., Bleuet, P., Borg, J., Bradley, J.P., Brearley, A., Brenker, F., Brennan, S., Bridges, J.C., Browning, N.D., Brucato, J.R., Bullock, E., Burchell, M.J., Busemann, H., Butterworth, A., Chaussidon, M., Cheuvront, A., Chi, M., Cintala, M.J., Clark, B.C., Clemett, S.J., Cody, G., Colangeli, L., Cooper, G., Cordier, P., Daghlian, C., Dai, Z., d'Hendecourt, L., Djouadi, Z., Dominguez, G., Duxbury, T., Dworkin, J.P., Ebel, D.S., Economou, T.E., Fakra, S., Fairey, S.A.J., Fallon, S., Ferrini, G., Ferroir, T., Fleckenstein, H., Floss, C., Flynn, G., Franchi, I.A., Fries, M., Gainsforth, Z., Gallien, J.-P., Genge, M., Gilles, M.K., Gillet, Ph., Gilmour, J., Glavin, D.P., Gounelle, M., Grady, M.M., Graham, G.A., Grant, P.G., Green, S.F., Grossemy, F., Grossman, L., Grossman, J.N., Guan, Y., Hagiya, K., Harvey, R., Heck, P., Herzog, G.F., Hoppe, P., Hörz, F., Huth, J., Hutcheon, I.D., Ignatyev, K., Ishii, H., Ito, M., Jacob, D., Jacobsen, C., Jacobsen, S., Jones, S., Joswiak, D., Jurewicz, A., Kearsley, A.T., Keller, L.P., Khodja, H., Kilcoyne, A.L.D., Kissel, J., Krot, A., Langenhorst, F., Lanzirotti, A., Le, L., Leshin, L.A., Leitner, J., Lemelle, L., Leroux, H., Liu, M.-C., Luening, K., Lyon, I., MacPherson, G., Marcus, M.A., Marhas, K., Marty, B., Matrajt, G., McKeegan, K., Meibom, A., Mennella, V., Messenger, K., Messenger, S., Mikouchi, T., Mostefaoui, S., Nakamura, T., Nakano, T., Newville, M., Nittler, L.R., Ohnishi, I., Ohsumi, K., Okudaira, K., Papanastassiou, D.A., Palma, R., Palumbo, M.E., Pepin, R.O., Perkins, D., Perronnet, M., Pianetta, P., Rao, W., Rietmeijer, F.J.M., Robert, F., Rost, D., Rotundi, A., Ryan, R., Sandford, S.A., Schwandt, C.S., See, T.H., Schlutter, D., Sheffield-Parker, J., Simionovici, A., Simon, S., Sitnitsky, I., Snead, C.J., Spencer, M.K., Stadermann, F.J., Steele, A., Stephan, T., Stroud, R., Susini, J., Sutton, S.R., Suzuki, Y., Taheri, M., Taylor, S., Teslich, N., Tomeoka, K., Tomioka, N., Toppani, A., Trigo-Rodríguez, J.M., Troadec, D., Tsuchiyama, A., Tuzzolino, A.J., Tyliszczak, T., Uesugi, K., Velbel, M., Vellenga, J., Vicenzi, E., Vincze, L., Warren, J., Weber, I., Weisberg, M., Westphal, A. J., Wirick, S., Wooden, D., Wopenka, B., Wozniakiewicz, P., Wright, I., Yabuta, H., Yano, H., Young, E.D., Zare, R.N., Zega, T., Ziegler, K., Zimmermann, L., Zinner, E., Zolensky, M., 2006. Comet 81P/Wild 2 under a microscope. Science 314, 1711–1716.

Crank, J., 1975. The Mathematics of Diffusion. Clarendon Press.

Domínguez, G., Westphal, A.J., Jones, S.M., Phillips, M.L.F., 2004. Energy loss and impact cratering in aerogels: theory and experiment. Icarus 172, 613–624.

Flynn, G.J., Bleuet, P., Borg, J., Bradley, J.P., Brenker, F.E., Brennan, S., Bridges, J., Brownlee, D.E., Bullock, E.S., Burghammer, M., Clark, B.C., Dai, Z.R., Daghlian, C.P., Djouadi, Z., Fakra, S., Ferroir, T., Floss, C., Franchi, I.A., Gainsforth, Z., Gallien, J.-P., Gillet, Ph., Grant, P.G., Graham, G.A., Green, S.F., Grossemy, F., Heck, P.R., Herzog, G.F., Hoppe, P., Hörz, F., Huth, J., Ignatyev, K., Ishii, H.A., Janssens, K., Joswiak, D., Kearsley, A.T., Khodja, H., Lanzirotti, A., Leitner, J., Lemelle, L., Leroux, H., Luening, K., MacPherson, G.J., Marhas, K.K., Marcus, M.A., Matrajt, G., Nakamura, T., Nakamura-Messenger, K., Nakano, T., Newville, M., Papanastassiou, D.A., Pianetta, P., Rao, W., Riekel, C., Rietmeijer, F.J.M., Rost, D., Schwandt, C.S., See, T.H., Sheffield-Parker, J., Simionovici, A., Sitnitsky, I., Snead, C.J., Stadermann, F.J., Stephan, T., Stroud, R.M., Susini, J., Suzuki, Y., Sutton, S.R., Taylor, S., Teslich, N., Troadec, D., Tsou, P., Tsuchiyama, A., Uesugi, K., Vekemans, B., Vicenzi, E.P., Vincze, L., Westphal, A.J., Wozniakiewicz, P., Zinner, E., Zolensky, M.E., 2006. Elemental compositions of comet 81P/Wild 2 samples collected by Stardust. Science 314, 1731–1735.

Hopfe, W.D., Goldstein, J.I., 2001. The metallographic cooling rate method revisited/application to iron meteorites and mesosiderites. Meteorit. Planet. Sci. 36, 135–154.

Hörz, F., Zolensky, M.E., Bernhard, R.P., See, T.H., Warren, J.L., 2000. Impact features and projectile residues in aerogel exposed on Mir. Icarus 147, 559–579.

Hörz, F., Bastien, R., Borg, J., Bradley, J.P., Bridge, J.C., Brownlee, D.E., Burchell, M.J., Chi, M., Cintala, M.J., Dai, Z.R., Djouadi, Z., Dominguez, G., Economou, T.E., Fairey, S.A.J., Floss, C., Franchi, I.A., Graham, G.A., Green, S.F., Heck, P., Hoppe, P., Huth, J., Ishii, H., Kearsley, A.T., Kissel, J., Leitner, J., Leroux, H., Marhas, K., Messenger, K., Schwandt, C.S., See, T.H., Snead, C., Stadermann, F.J., Stephan, T., Stroud, R., Teslich, N., Trigo-Rodríguez, J.M., Tuzzolino, A.J., Troadec, D., Tsou, P., Warren, J., Westphal, A., Wozniakiewicz, P., Wright, I., Zinner, E., 2006. Impact features on Stardust: implications for Comet 81P/Wild 2 dust. Science 314, 1716–1719.

Hudon, P., Baker, D.R., 2002. The nature of phase separation in binary oxide melts and glasses. I. Silicate systems. J. Non-Cryst. Solids 303, 299–345.

Ishii, H.A., Bradley, J.P., Dai, Z.R., Chi, M., Kearsley, A.T., Burchell, M.J., Browning, N.D., Molster, F., 2008. Comparison of Comet 81P/Wild 2 dust with interplanetary dust from comets. Science 319, 447–450.

Keller, H., Schwerdtfeger, K., Petri, H., Hennesen, K., 1979. Tracer diffusivity of ^{45}Ca and electrical conductivity in calcium oxide-silica melts. Metall. Trans. B10, 67–70.

Lacks, D.L., Rear, D.B., Van Orman, J.A., 2007. Molecular dynamics simulation of viscosity, chemical diffusivities and partial molar volumes of liquids along the $MgO–SiO_2$ join as functions of pressure. Geochim. Cosmochim. Acta 71, 1312–1323.

LaTourette, T., Wasserburg, G.J., Fahey, A.J., 1996. Self diffusion of Mg, Ca, Ba, Nd, Yb, Ti, Zr, and U in haplobasaltic melt. Geochim. Cosmochim. Acta 60, 1329–1340.

Leko, V.K., Gusakova, N.K., Mescheryakova, E.V., Prokhorova, T.I., 1977. The effect of impurity alkali oxides, hydroxyl groups, Al_2O_3, and Ga_2O_3 on the viscosity of vitreous silica. Sov. J. Glass Phys. Chem. 3, 204–210.

Leroux, H., Rietmeijer, F.J.M., Velbel, M.A., Brearley, A.J., Jacob, D., Langenhorst, F., Bridges, J.C., Zega, T.J., Stroud, R.M., Cordier, P., Harvey, R.P., Lee, M., Gounelle, M., Zolensky, M.E., in press. A TEM study of thermally modified Comet 81P/Wild 2 dust particles by interactions with the aerogel matrix during the Stardust capture process. Meteorit. Planet. Sci. 43, 97–120.

Marty, B., Palma, R.L., Pepin, R.O., Zimmermann, L., Schlutter, D.J., Burnard, P.G., Westphal, A.J., Snead, C.J., Bajt, S., Becker, R.H., Simones, J.E., 2008. Helium and neon abundances and compositions in cometary matter. Science 319, 75–78.

Mysen, B.O., Richet, P., 2005. Silicate Glasses and Melts, Properties and Structure. Elsevier, pp. 169–198.

Noguchi, T., Nakamura, T., Okudaira, K., Yano, H., Sugita, S., Burchell, M.J., 2007. Thermal alteration of hydrated minerals during hypervelocity capture to silica aerogel at the flyby speed of Stardust. Meteorit. Planet. Sci. 42, 357–372.

Pertermann, M., Whittington, A.G., Hofmeister, A.M., Spera, F.J., Zayak, J., in press. Transport properties of low-sanidine single-crystals, glasses and melts at high temperature. Contrib. Mineral.

Rietmeijer, F.J.M., Nakamura, T., Tsuchiyama, A., Uesugi, K., Nakano, T., Leroux, H., in press. Origin and formation of iron-silicide phases in the aerogel of the Stardust mission. Meteorit. Planet. Sci. 43, 121–134.

Sandford, S.A., Aléon, J., Alexander, C.M.O'D., Araki, T., Bajt, S., Baratta, G.A., Borg, J., Bradley, J.P., Brownlee, D.E., Brucato, J.R., Burchell, M.J., Busemann, H., Butterworth, A., Clemett, S.J., Cody, G., Colangeli, L., Cooper, G., d'Hendecourt, L., Djouadi, Z., Dworkin, J.P., Ferrini, G., Fleckenstein, H., Flynn, G.J., Franchi, I.A., Fries, M., Gilles, M.K., Glavin, D.P., Gounelle, M., Grossemy, F., Jacobsen, C., Keller, L.P., Kilcoyne, A.L.D., Leitner, J., Matrajt, G., Meiborn, A., Mennelle, V., Mostefaoui, S., Nittler, L.R., Palumbo, M.E., Papanastassiou, D.A., Robert, F., Rotundi, A., Snead, C.J., Spencer, M.K., Stadermann, F.J., Steele, A., Stephan, T., Tsou, P., Tyliszczak, T., Westphal, A.J., Wirick, S., Wopenka, B., Yabuta, H., Zare, R.N., Zolensky, M.E., 2006. Organics captured from Comet 81P/Wild 2 by the Stardust Spacecraft. Science 314, 1720–1724.

Snyder, D., Gier, E., Carmichael, I., 1994. Experimental determination of the thermal conductivity of molten $CaMgSiO_6$ and the transport of heat through magmas. J. Geophys. Res. 99, 503–516.

Toplis, M.J., Dingwell, D.B., Hess, K.-U., Lenci, T., 1997. Viscosity, fragility, and configurational entropy of melts along the join SiO_2–$NaAlO_2$. Am. Mineral. 82, 979–990.

Urbain, G., Bottinga, Y., Richet, P., 1982. Viscosity of liquid silica, silicates and aluminosilicates. Geochim. Cosmochim. Acta 46, 1061–1072.

Van Cappellen, E., 1990. The parameterless correction method in X-ray microanalysis. Microsc. Microanal. Microstruct. 1, 1–22.

Van Cappellen, E., Doukhan, J.C., 1994. Quantitative transmission X-ray microanalysis of ionic compounds. Ultramicroscopy 53, 343–349.

Westphal, A.J., Snead, C., Butterworth, A., Graham, G.A., Bradley, J.P., Bajt, S., Grant, P.G., Bench, G., Brennan, S., Pianetta, P., 2004. Aerogel keystones: extraction of complete hypervelocity impact events from aerogel collectors. Meteorit. Planet. Sci. 39, 1375–1386.

Zolensky, M.E., 2005. Extraterrestrial water. Elements 1, 39–43.

Zolensky, M.E., Zega, T.J., Yano, H., Wirick, S., Westphal, A.J., Weisberg, M.K., Weber, I., Warren, J.L., Velbel, M.A., Tsuchiyama, A., Tsou, P., Toppani, A., Tomioka, N., Tomeoka, K., Teslich, N., Taheri, M., Susini, J., Stroud, R., Stephan, T., Stadermann, F.J., Snead, C.J., Simon, S.B., Simionovici, A., See, T.H., Robert, F., Rietmeijer, F.J.M., Rao, W., Perronnet, M.C., Papanastassiou, D.A., Okudaira, K., Ohsumi, K., Ohnishi, I., Nakamura-Messenger, K., Nakamura, T., Mostefaoui, S., Mikouchi, T., Meibom, A., Matrajt, G., Marcus, M.A., Leroux, H., Lemelle, L., Le, L., Lanzirotti, A., Langenhorst, F., Krot, A.N., Keller, L.P., Kearsley, A.T., Joswiak, D., Jacob, D., Ishii, H., Harvey, R., Hagiya, K., Grossman, L., Grossman, J.N., Graham, G.A., Gounelle, M., Gillet, P.h., Genge, M.J., Flynn, G., Ferroir, T., Fallon, S., Ebel, D.S., Dai, Z.R., Cordier, P., Clark, B., Chi, M., Butterworth, A.L., Brownlee, D.E., Bridges, J.C., Brennan, S., Brearley, A., Bradley, J.P., Bleuet, P., Bland, P.A., Bastien, R., 2006. Mineralogy and petrology of comet 81P/Wild 2 nucleus samples. Science 314, 1735–1739.